Trans R Soc Trop Med Hyg 2025; **0**: 1–12
https://doi.org/10.1093/trstmh/traf070 Advance Access publication 0 2025

Remoscope: a label-free imaging cytometer for malaria diagnostics

Paul M. Lebel [a,*], Ilakkiyan Jeyakumar [a], Michelle W. L. Khoo [a,†], James Emorut [b,†], Chris Charlton [a,†], Aditi Saxena [a,‡], Axel Jacobsen [a,§], Emily Huynh [a,¶], William Wu [a,‖], Greg Courville [a], Pei-Chuan Fu [a,], Madhura Raghavan [c], Robert Puccinelli [d], Peter Olwoch [b], Grant Dorsey [e], Philip J. Rosenthal [e], Joseph DeRisi [a,c], and Rafael Gomez-Sjoberg [a]**

[a]Department of Bioengineering, Chan Zuckerberg Biohub San Francisco, 499 Illinois Street, San Francisco, CA 94158, USA; [b]Department of Laboratory Medicine, Infectious Disease Research Collaboration, 2C Nakasero Hill Road, 10106, Uganda; [c]Department of Biochemistry and Biophysics, University of California, San Francisco, 600 16th street, San Francisco, CA 94158, USA; [d]Department of Bioengineering, University of California , Berkeley, Stanley Hall University Drive, Berkeley, CA 94720, USA; [e]Department of Medicine, University of California, San Francisco, San Francisco, CA 94158, USA

[*]Corresponding author: Tel: 415-549-3300; E-mail: paul.lebel@czbiohub.org
[†]These authors contributed equally.
[‡]Present address: Harvard T.H. Chan School of Public Health.
[§]Present address: Neuralink.
[¶] Present address: University of Pennsylvania, Philadelphia, PA.
[‖]Present address: Tezerakt LLC at Google.
[**]Present address: Liminal Insights.

Received 12 February 2025; revised 23 April 2025; editorial decision 13 June 2025; accepted 23 June 2025

Background: Malaria diagnostic testing remains a burden on healthcare systems. Here we present Remoscope, a portable imaging cytometer that scans fresh, unstained whole blood using a custom neural network running on low-cost hardware. Remoscope performs label-free, quantitative, stage-specific detection of *Plasmodium falciparum* (*Pf*) by screening up to 2 million red blood cells (RBCs) in 1–12 min, without sample fixation, staining or slide scanning. Low-cost disposable cartridges are used to confine flowing blood to an ultrathin sheet for imaging.

Methods: Performance was benchmarked in vitro by titration of cultured *Pf* (17.1–710 000 parasites/µl) into whole blood. A study of Remoscope's diagnostic accuracy was evaluated in a cohort of 500 individuals in eastern Uganda, comprising 601 unique clinic visits. Parallel measurements of parasitaemia were performed using Remoscope, quantitative polymerase chain reaction (qPCR) and thick blood smears.

Results: Clinically, Remoscope's 10× diluted blood assay had a limit of detection with respect to qPCR of 95.1 parasites/µl, sensitivity of 83%, specificity of 96%, positive predictive value of 91% and negative predictive value of 93%.

Conclusions: Remoscope's speed, accuracy, cost and ease of use address key challenges in malaria diagnosis worldwide. In this pilot study, the diagnostic accuracy approaches that of expert thick smears performed in duplication.

Keywords: AI, diagnostics, global health, label-free, low-cost, malaria

Introduction

Malaria's annual death toll of >600 000 people disproportionately affects low-income regions with limited access to healthcare. Despite decades of attempts to control the disease, the number of malaria cases has steadily increased globally since 2020, with most new cases appearing in the World Health Organization Africa region.[1] In addition to the emergence and spread of drug-resistant parasites and insecticide-resistant vectors, the recent arrival of the *Anopheles stephensi* mosquito in Africa[1,2] has begun driving drug and diagnosis-resistant infections upwards in more densely populated urban areas, and with it, the potential for growing disease and diagnostic burden.[3] Although light

microscopy of stained blood smears has remained the gold standard diagnostic for more than a century,[4–6] the dependence on skilled human labour imposes limitations on accessibility. This leaves underresourced facilities unable to cope with the daily diagnostic burden, resulting in missed cases, delayed turnaround time and/or poor diagnostic accuracy.[7] Immunochromatographic assays identifying specific antigens (rapid diagnostic tests [RDTs]) are a cost-effective modality but are not quantitative and are susceptible to histidine-rich protein 2 (HRP2) deletions in the *Plasmodium falciparum* (*Pf*) genome.[1,8] Additionally, HRP2-based RDTs remain positive for variable durations after treatment,[9,10] failing to discriminate live parasites from residual circulating antigen. Although molecular technologies such as polymerase chain reaction (PCR), loop-mediated isothermal amplification and recombinase polymerase and loop-mediated isothermal amplification methods are highly sensitive,[11–16] they depend on cold chains and their cost remains too high for routine use in endemic countries. These issues highlight the need for novel approaches to address the ongoing diagnostic burden.

Many recent efforts have leveraged machine learning combined with automated slide-scanning microscopes[17–21] to reduce the inspection burden on technicians. While these efforts retain the quantitative advantages of traditional microscopy, many systems require manual smear preparation,[17–19] and with it, the corresponding variability in smear quality and dependence on reagents, which contribute to limitations in accuracy and delayed turnaround time. A fully automated commercial slide staining and scanning system was recently developed[20] but is not yet available to malaria-endemic countries, leaving the vast majority of cases unaddressed.

Here we describe Remoscope, a label-free imaging cytometer that was designed to meet the diagnostic needs of malaria-endemic regions. It performs real-time morphological analysis on up to 2 million red blood cells (RBCs) in <12 min, for approximately US$1 per test (Figure 1, Supplementary Figure 1 and Supplementary Video 1). The overall dimensions are approximately 200×200×300 mm, accommodating labs with limited working space. The cost of the current research prototype is US$2000. It uses disposable, ultrathin flow cartridges (see Supplementary Note 1 for fabrication details) to confine fresh, unstained whole blood in a monolayer suitable for single-cell imaging (similar to a thin smear in motion), despite their high concentration at 35–51% haematocrit.[22] Operation of the system requires minimal training due to automation, which is achieved by stabilizing the focus, illumination level and flow rate using feedback (Figure 1b). Parasites are identified (see Figure 2 for examples) in real time by You Only Glance Once (YOGO), a custom convolutional neural network for cell detection and classification, allowing the system to monitor the density of cells in the chamber and display live parasitaemia estimates during the run. Details of the open-source instrument control software are provided in Supplementary Figure 2, described in the Methods and published on GitHub (see Code Availability).

In contrast with other methods, it does not require sample pre-processing aside from anticoagulation with ethylenediaminetetraacetic acid (EDTA), enabling the screening process to begin soon after the blood draw. Real-time analysis permits early termination once the statistics meet a threshold, usually <1 min for highly parasitized blood (see Supplementary Figures 3 and 4). However, because the clinically relevant range of parasitaemia spans many orders of magnitude,[12] it is helpful for a malaria test to be quantitative and to express bounds of uncertainty. Onboard statistical analysis accounts for both stochastic sampling error as well as removal of systematic bias in cell classification, enabling results that are operator independent.

In this work, we quantify Remoscope's performance on in vitro cultured *Pf* (Figure 3) as well as in a prospective study of diagnostic accuracy on a cohort of individuals in eastern Uganda (Figure 4), comparing its performance with expert-level thick blood smears as well as qPCR. We also demonstrate its ability to distinguish drugged from undrugged *Pf* parasites using an in vitro half-maximal effective concentration (EC_{50}) assay with chloroquine (CQ).

Methods

The supplementary materials describe technical details of the study's index test. The Remoscope design, cartridge fabrication, model training and software details can all be found in Supplementary Note 1: Remoscope technical methods. The parasite annotation strategy is described in detail in Supplementary Note 2: Annotation guide. Analysis methods used for uncertainty calculations are found Supplementary Note 3: Statistical analysis and error estimation.

In vitro validation methods

Parasite culture

Pf strains W2 and NF54 were cultured in either T-25, T-75 or T-150 flasks depending on the scale of experimentation. Cultures were grown in complete RPMI ($RPMI_c$) supplemented with 0.5% Albumax II (catalogue no. 11021029; Gibco Life Sciences, Carlsbad, CA, USA), 2 g/l sodium bicarbonate, 0.1 mM hypoxanthine, 25 mM HEPES (pH 7.4) and 50 µg/l gentamicin. Cells were maintained at 2% haematocrit in a gas- and temperature-controlled environment set to 37°C, 5% O_2 and 5% CO_2. To avoid parasite overgrowth and death, cultures were split and passaged daily to maintain parasitaemia of 1–5%.

*Thin blood smear preparation and counting for **in vitro** validation*

The 500 µl of culture were centrifuged and 10 µl of the pellet was used to create a thin smear on a glass specimen slide. To visualize infected RBCs, slides were dried, fixed in methanol and stained for 15 min using 2% Giemsa. The slide was then observed at 100× magnification on an upright light microscope.

Enrichment of specific life-stages

The *Pf* life cycle under culture conditions contained a mixture of life cycle stages, depending on the degree of synchronization. To aid in the annotation effort, specific stages were enriched in order to increase the density of image data.

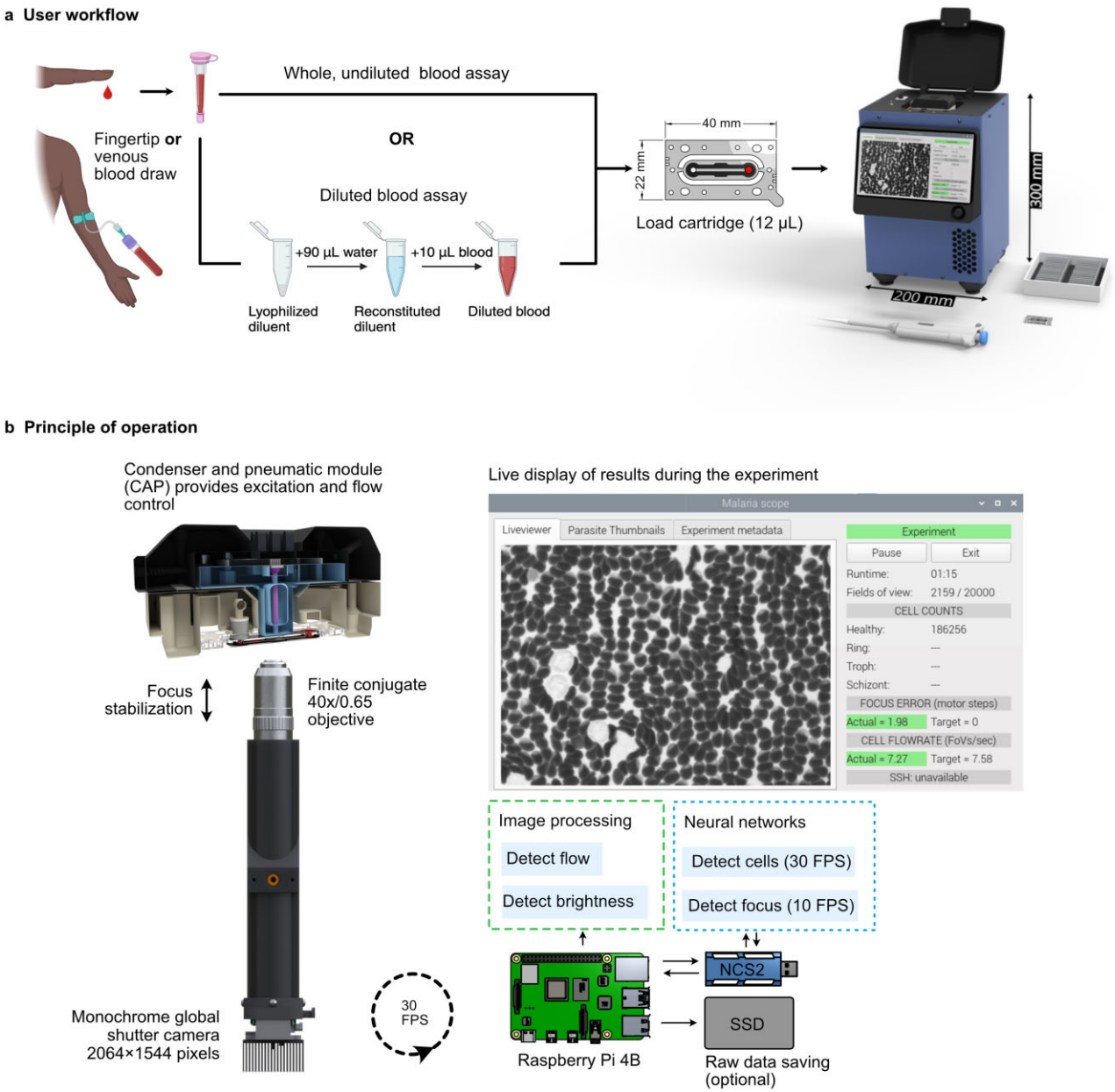

Figure 1. Overview of Remoscope's workflow and principle of operation. **(a)** The user workflow consists of a blood draw (either fingertip or venous, with EDTA anticoagulation), followed by an optional dilution step, chamber loading, metadata entry, run start and monitoring for completion (1–12 min). **(b)** High-level overview of the system processes. During continuous image acquisition, the rate of blood flow and image brightness are monitored by classical image processing on the Raspberry Pi, while focal position and cell detection are both performed using neural networks executed on the Neural Compute Stick 2 (NCS2). Intermediate results are updated and displayed to the user throughout the course of the experiment, while focus, brightness and flow rate are stabilized using feedback. During the run, the statistics of the parasite counts are updated once per second, triggering the end of the experiment if the stop conditions are met. Raw data can optionally be saved to an SSD during the experiment.

Sorbitol synchronization—enrichment of ring-stage parasites A total of 50 ml of culture at >10% rings was moved into a 50-ml falcon tube and centrifuged for 5 min at 1500 rpm with low brake. All but 5 ml of media and RBCs were aspirated and mixed gently with an equal volume of warm 5% sorbitol. The tube was shaken slowly to mix every 5 min for 15 min and then centrifuged again for 5 min at 1500 rpm with low brake. The media and sorbitol were aspirated completely and the pellet was resuspended in the starting volume of $RPMI_c$.

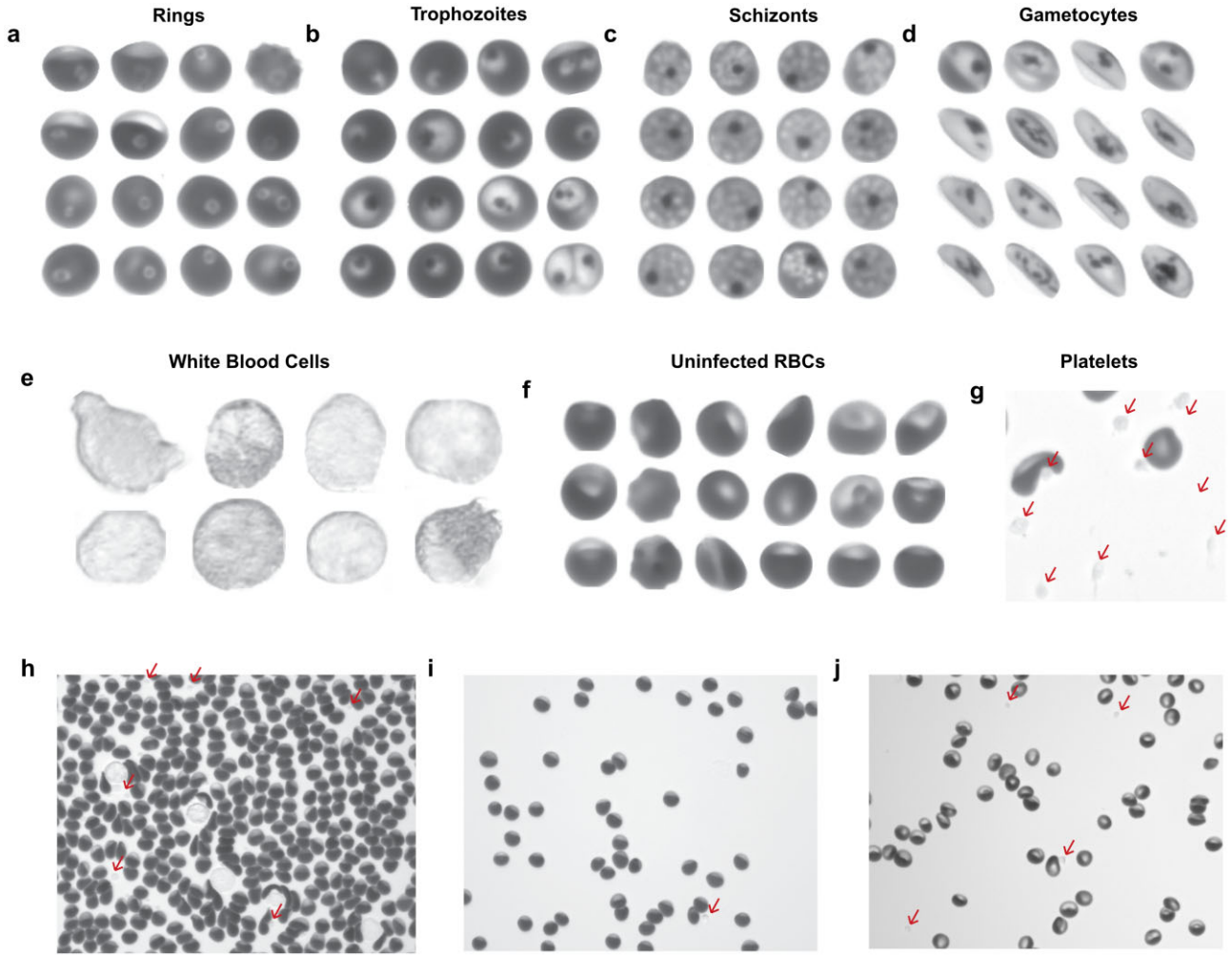

Figure 2. Examples of label-free blood cell images classified by Remoscope. **(a)** Ring-infected RBCs of various submorphologies including amoeboid, dendritic and canonical rings. **(b)** Trophozoite-infected RBCs of various submorphologies including early trophozoites, late trophozoites and multiply-infected RBCs (upper and lower right). **(c)** Schizont-infected RBCs showing partial and full merozoite segmentation. **(d)** Gametocytes, ranging from stage 3 to 5. Stage 1 and 2 gametocytes were not distinguished from trophozoites due to a lack of sufficiently unique features. **(e)** White blood cells. **(f)** Uninfected RBCs exhibiting a variety of morphologies. **(g)** A region of interest with a high density of platelets, which are called out with red arrows in panels g–j. **(h)** A complete field of view containing uninfected, undiluted blood under flow. RBCs are seen with shear distortion features such as rarified trailing edges. **(i)** A complete field of view containing uninfected RBCs diluted to 5% haematocrit, with normal haemoglobin content. **(j)** A complete field of view containing diluted blood at 5% haematocrit, exhibiting low haemoglobin pigmentation.

Purification—enrichment of trophozoite- and schizont-stage parasites Magnetic-activated cell sorting (MACS) purification was carried out as described previously.[23] Cultures were first synchronized at the ring stage and then MACS purified once at >10% parasitaemia in the late-trophozoite stage. Then 50-ml cultures were centrifuged at 1500 rpm for 5 min and the supernatant was aspirated until 20 ml remained. Four LD columns (catalogue no. 130-042-901; Miltenyi Biotec, Bergisch Gladbach, Germany) were washed twice with $RPMI_c$ and washed with 5 ml of resuspended culture. With 1 ml remaining, an additional 5 ml of $RPMI_c$ was added to wash the columns. The columns were eluted with 5 ml of $RPMI_c$. The eluate was used to expand the culture or used in experiments.

Titration and flow cytometric analysis of parasitaemia

Parasitaemia assessment was performed on a serial twofold dilution of in vitro *Pf* culture into type-matched fresh, healthy, whole blood. Identical aliquots of culture run on Remoscope were also assessed by flow cytometry. Cells were diluted to 0.5% haematocrit and fixed in 2% paraformaldehyde for 1 h at room temperature in a 96-well U-bottom cell culture plate. The fixed cells were then stained overnight in 50 nM of YOYO-1 and run using a high-throughput system attachment on a FACSCelesta flow cytometer (Becton Dickinson, Franklin Lakes, NJ, USA). Each sample was run in duplicate, with a collection threshold of 2 million events. Gating and parasitaemia calculations were then carried out using FlowJo (Becton Dickinson).

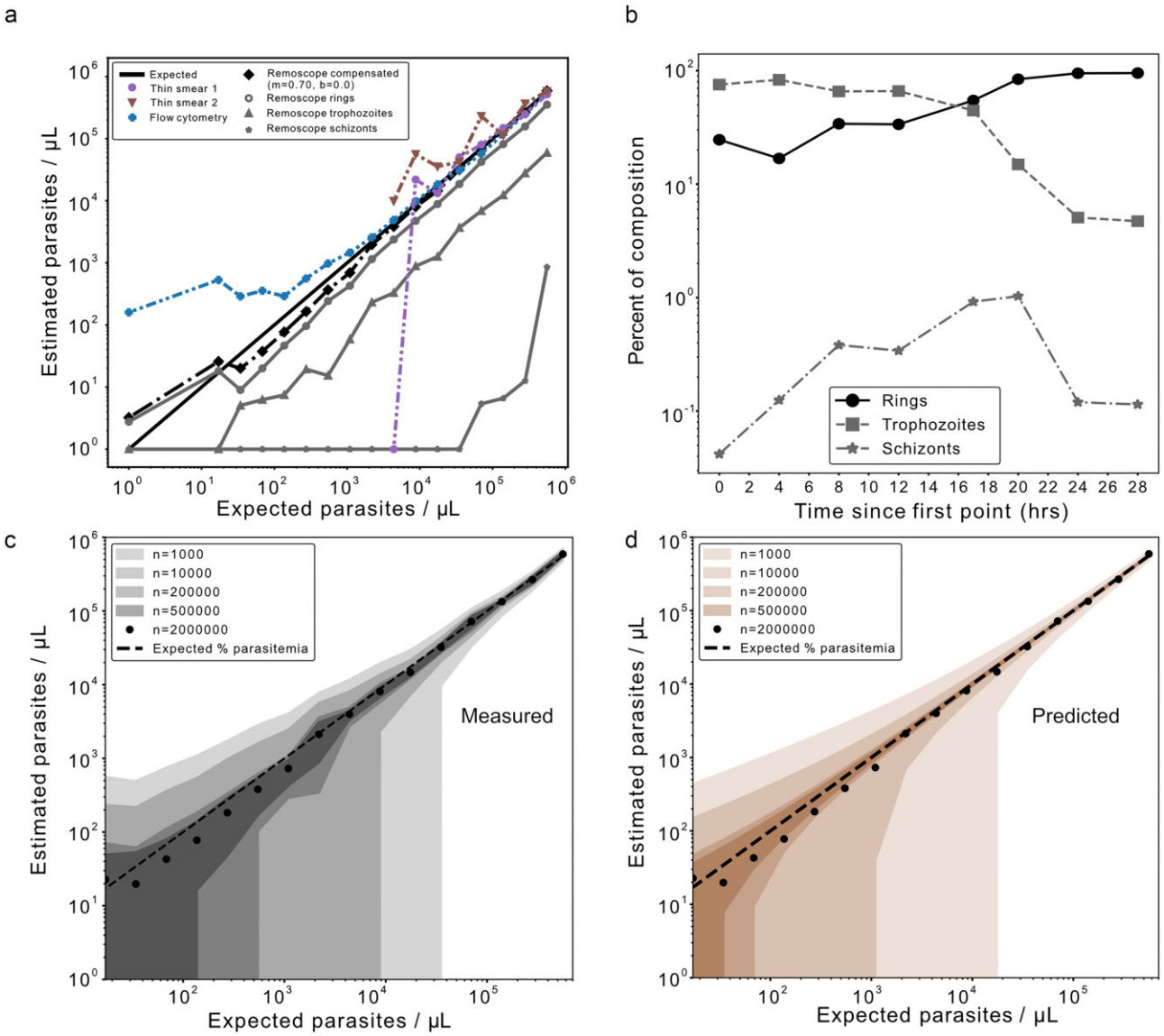

Figure 3. Remoscope performance on lab-cultured *Pf*. **(a)** Life stage–specific parasitaemia quantification over a 16-point serial dilution of parasite culture into uninfected, undiluted whole blood. Remoscope results are shown with black and grey markers. Thin smear microscopy counting approximately 1000 cells per point are shown for the first eight titration points only, and flow cytometry (2×10^6 events/point) are plotted as blue '+' signs. Remoscope data have undergone linear transformation with parameters m=0.7 and b=0. **(b)** Parasite life stage time course experiment over a continuous 28-h period showing the assessed fractional compositions of each asexual life stage in the culture as a function of time. **(c)** Uncertainty quantification of the titration data as a function of the number of cells analysed. Contour regions span the overall mean±1 SD across data subsampled at the indicated number of cells. **(d)** Theoretical prediction of the experimental uncertainty shown in (c), as described in Supplementary Note 3.

Gametocyte induction strategy

Freshly thawed strains of NF54 were utilized to ensure the maximal capacity of gametocytogenesis and blood <1 week old was used to minimize lysis of cells during the induction assay. Cultures were grown in $RPMI_c$ and synchronized using sorbitol and MACS purification. On day −3, a T-150 was set up with 2% trophozoites at 5% haematocrit at a total volume of 25 ml. On day −2, haematocrit was lowered 1:2 by adding 25 ml of fresh media. On day −1, half the media was exchanged with $RPMI_c$ and the culture was split to approximately 2% trophozoites. Subsequently, daily media changes were carried out with no addition of new blood. The culture was smeared daily, until stage IV or V gametocytes were observed.

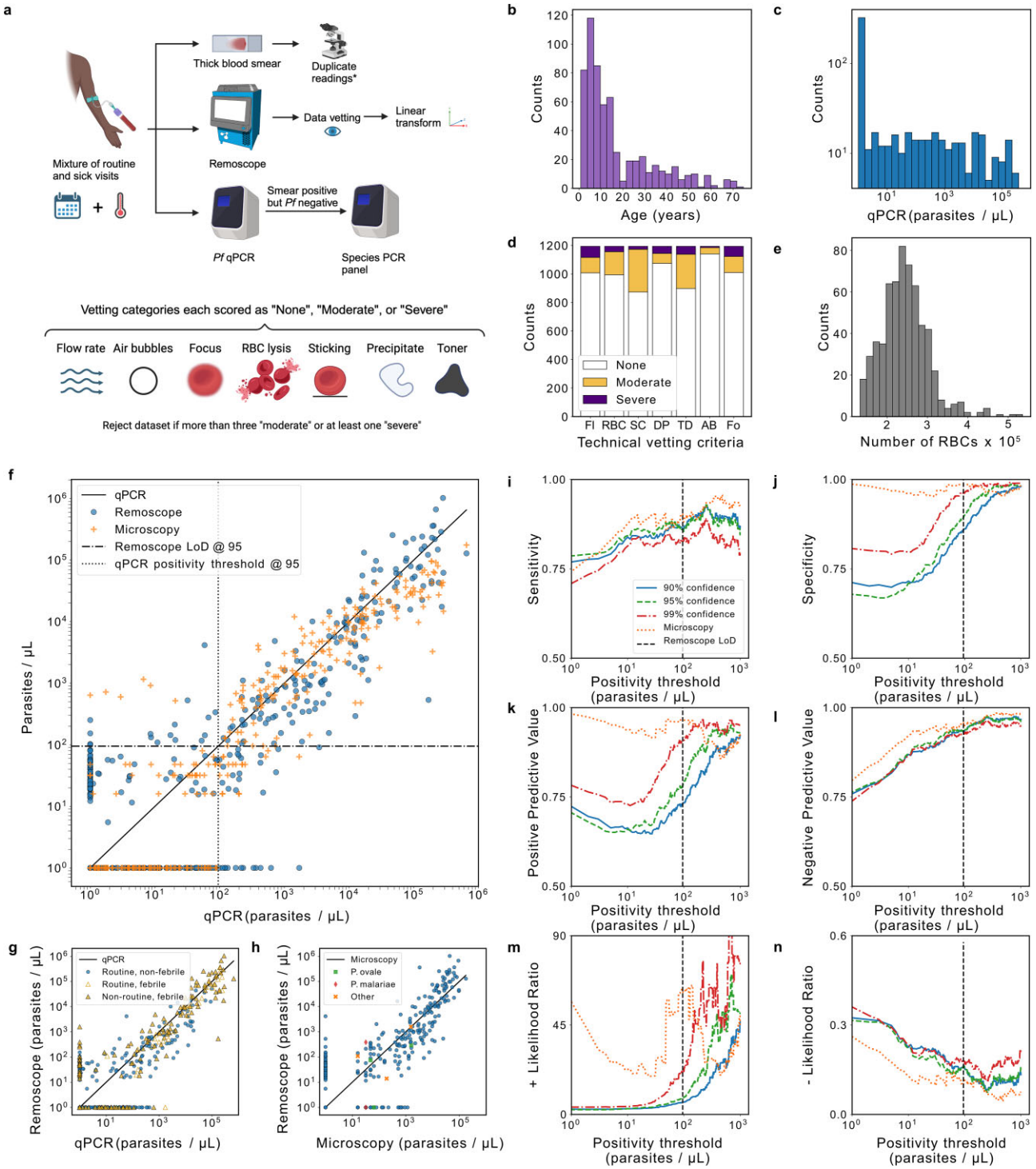

Figure 4. Clinical study in a Ugandan cohort using 10× diluted blood. **(a)** Overall data collection and vetting strategy: venous blood samples were sent to Remoscope, qPCR and thick blood smear microscopy with duplicate readings. Remoscope datasets underwent a quality vetting process to discard low quality datasets due to technical failures, according to seven vetting criteria. A linear transformation (slope and offset correction) was used to adjust for the average recall and false positive rates. **(b)** Histogram of participant ages. **(c)** Histogram of cohort parasitaemias by qPCR. **(d)** Stacked histogram of Remoscope dataset vetting results. Fl: flow rate; RBC: RBC integrity; SC: stuck cells; DP: diluent precipitate; TD: toner and debris; AB: air bubbles; Fo: focus quality. **(e)** Histogram of total RBC counts per experiment in the cohort (diluted blood), after filtering for N>132 735 cells

Figure 4. Continued. (bottom 5% removed). **(f)** Comparison of Remoscope and microscopy against qPCR. The horizontal dashed line indicates the computed Remoscope LoD. The vertical dotted line indicates the corresponding threshold on the qPCR axis. The two lines partition the plot into true negatives (lower left), true positives (upper right), false positives (upper left) and false negatives (lower right). **(g)** The same Remoscope data as in (f), but plotted with delineation of visit type and febrility status. **(h)** Direct comparison of Remoscope with microscopy. Non-*falciparum Plasmodium* species are denoted by distinct markers. 'Other' refers to samples testing positive by microscopy but negative for both *Pf* PCR as well as the species PCR panel. **(i)** Sensitivity, **(j)** specificity, **(k)** PPV, **(l)** NPV, **(m)** +LR and **(n)** −LR of the diagnostic test as a function of a common swept positivity threshold. Performance metrics were computed for three confidence thresholds: 0.9, 0.95 and 0.99. Linear transformation parameters were computed independently for each confidence threshold. In all subpanels, parasitaemia values were clipped to 1 parasite/µl.

Time course acquisition of life stages

The culture was twice synchronized by sorbitol treatment and the first time point was at the early trophozoite stage. Samples were prepared by spinning down culture at 2% haematocrit, resuspending the pellet in an equal volume of diluent to bring the haematocrit to approximately ∼50%. Images were acquired in full length runs every 4 h for 28 h.

Clinical study methods

We include responses to the Standards for Reporting of Diagnostic Accuracy Studies checklist in Supplementary Note 4.

Cohort description

We describe a prospective clinical study whose cohort is a subset of the Program for Resistance, Immunology, Surveillance, and Modeling of Malaria in Uganda (PRISM) Border Cohort study. All details on participant selection, visit schedule and eligibility can be found in Kamya et al.[24] The size of our analysed subset exceeds the number necessary for a confidence interval width of 5% (d), with an assumed sensitivity (Se) and specificity of 90% and a Z-score of 1.96, as computed using the method of Burderer[25]:

$$n = \frac{Z^2 Se\,(1 - Se)}{d^2} = \frac{1.96^2 0.9\,(1 - 0.9)}{0.05^2} = 139.$$

This study includes 226 microscopy-positive participants and 375 microscopy-negative participants.

Participant selection criteria

The study plan was to process all routine participants according to the PRISM border cohort's pre-existing visit schedule, up to a maximum of 1 000 runs, limited by the total number of available flow cartridges. Exceptions were made only in the event of Remoscope hardware or software down time and flow cartridge availability or technical failures. Sick visits, included to enrich prevalence, were sampled based on participants' presentation at the clinic with malaria symptoms and the ability to process the samples on Remoscope within a 24-h window. The absence of sampling bias can be inferred from Figure 4c, which shows a uniform random distribution of parasitaemia levels across many orders of magnitude.

Vetting process for data quality control

Datasets underwent a vetting process to remove technical failures. All videos from the study were exported to a directory and inspected without knowledge of parasitaemia or other participant metadata. The categories were scored as 'normal', 'moderate' or 'unusable' (flow issues, RBC abnormalities, cell sticking, diluent insolubility, debris, air bubbles or focus). If one or more categories were marked as 'unusable' or if three or more were marked as 'moderate', the dataset was rejected. Supplementary Figure 5 shows a graphical representation of the vetting status results for all clinical data.

Test procedures and sample preparation

Samples were processed on Remoscope within 24 h of the routine or sick visit blood draws after storage at room temperature. Fresh whole blood was mixed with diluent at a ratio of 1:10, comprising 10 mg/ml bovine serum albumin (catalogue no. A4737; Sigma-Aldrich, St. Louis, MO, USA), 10 mg/ml Tetronic 90R4 (catalogue no. 435546; Sigma-Aldrich) and 5 mM EDTA in Dulbecco's phosphate-buffered saline (DPBS). A total of 15 µl of diluted blood was loaded into a Remoscope flow cartridge and placed in the instrument. A total of 20 000 full image runs were completed for each participant without ending early. Raw data were saved to solid-state drives (SSDs) and processed offline. YOGO was run on each image and processed as described in Supplementary Note 1. Thick smear microscopy and qPCR was also performed exactly as described in Kamya et al.[24]

Model training and test partitions

YOGO was trained on a partition of data consisting of local healthy donors, in vitro cultured *Pf* and a held-out subpartition of clinical data consisting of 1% of images from the top 20 highest parasitaemia cases (200 of 20 000 images) and approximately 1% of images taken from each of 98 healthy Ugandan participants. All images used for training/validation were excluded from the study. Inclusion of clinical parasites in the training dataset was found to improve model recall (the fraction of true parasites identified as such). Likewise, inclusion of a greater diversity of healthy data from the cohort was found to reduce model false positive rates. For more detail, see Supplementary Note 1.

Results

Performance assessments using cultured parasites

First, we tested Remoscope's limit of detection (LoD) with a serial dilution of cultured parasites into uninfected whole blood. By spiking lab-cultured *Pf* into healthy, undiluted whole blood, we were able to vary parasitaemia over a wide range, providing extrinsic validation of whether YOGO models trained on human annotations (Table 1) were able to assess parasitaemia levels (Supplementary Videos 2–17). We saw a linear response over a 16-point serial dilution into whole blood from a starting

Table 1. Summary of fully annotated cell classes used for model fine tuning.

Class	Cultured *Pf*	Clinical cohort	Malaria-free region	Total
Uninfected RBCs	5193	1 616 810	4 375 116	5 997 119
Rings	20 700	1507	0	22 207
Trophozoites	8507	274	0	8781
Schizonts	341	0	0	341
Gametocytes	127	0	0	127

The total number of annotated cells of each category is listed for each of three separate sources: a lab-cultured W2 strain of *Pf*, a Ugandan clinical cohort and blood donated from a malaria-free region. We define fully annotated as (a) every cell has been annotated by a human, (b) a malaria-free donation source (all RBCs assigned en masse as healthy/uninfected) or (c) a holdout 'train' partition of images from the Ugandan cohort that were all double-negative by both qPCR and microscopy assigned en masse as healthy/uninfected. All parasite class counts listed above were human annotated either in Label Studio or by the thumbnail annotation described above and in the Methods section.

parasitaemia of 11.2%, as determined by thin smear Giemsa microscopy performed by three independent readers (Figure 3). Each dilution point was additionally screened using conventional flow cytometry and thin blood smears for comparison. We acquired approximately 2 million events per condition using flow cytometry and found that the sensitivity/specificity trade-off was inferior to Remoscope's. Thin blood smears, although highly specific, were ineffective at low parasitaemia due to inadequate sampling power when counting approximately 1000 RBCs per condition. Therefore, only the first eight titration points were counted manually, as the remaining points had fewer than one parasite per 1000 RBCs.

Compensated Remoscope measurements remained linear down to 0.00034% parasitaemia (17.1/µl equivalent), with a root mean square ratiometric error of 0.29 over the entire range. Model confidence thresholding was explored during analysis to vary the trade-off between parasite recall and false positive rate (Supplementary Figure 6), resulting in an optimal value of 0.75. It should be noted that for rapid turnaround, the experiment can be set to terminate early upon achieving a target relative signal:noise ratio. For example, at 1000 parasites/µl (0.02% parasitaemia) with undiluted blood, 3 min of run time results in a Poisson error of $<$10% relative uncertainty.

We investigated the effect of throughput (number of cells) on the empirical error bounds by subsampling the titration datasets at n=1000, 10 000, 200 000, 500 000 and 2 000 000 cells per run (Figure 3b). We computed the standard deviation (SD) in estimated parasitaemia levels between subsampled datasets and plotted the mean±1 SD for each subsampling level. The effect of Poisson-limited counting statistics manifests as an inverse correlation between uncertainty bounds and the number of cells. The basal uncertainty in the data quantifies the number of cells required to resolve a given parasitaemia level.

We assessed discrimination of parasite life stages by conducting a synchronized time course using Remoscope to assess fractional compositions as a function of time. Throughout 28 h (beginning with a trophozoite-dominated culture), the ratio of rings to trophozoites was seen to cross over, while schizonts (defined as having segmented intraerythrocytic merozoites; see Supplementary Note 2) peaked thereafter. We note that while schizonts could be observed on Remoscope, their recall was low, presumably related to their cytoadherent properties.[26,27]

Table 2. Summary of participant visit types.

Visit types	Routine	Non-routine	Total
Febrile	53	194	247
Non-febrile	354	0	354
Totals	407	194	601

Numbers include participant visits passing all quality control vetting criteria. Participants with sickle cell disease or testing positive for other *Plasmodium* species were also withheld from analysis.

The ability to distinguish drug-treated from healthy parasite morphologies is also an important application in both laboratory and clinical settings. In the former, evaluating drug efficacies with an automated, label-free platform would serve to accelerate drug development. In the clinic, assessment of treatment efficacy is needed to distinguish active from treated infections, which RDTs and other molecular tests fail to provide.[9,10] In Supplementary Note 5, Remoscope was used to quantify the EC_{50} for CQ.

Diagnostic accuracy in a Ugandan cohort

Testing Remoscope in a clinical setting was central to evaluating its utility as a diagnostic tool, complete with real-world challenges. We deployed three Remoscopes for testing with a cohort of 500 individuals in eastern Uganda from January to September 2023. As part of the broader PRISM Border Cohort study,[24] participants were scheduled for routine monthly blood draws regardless of symptoms (Figure 4a). Additionally, non-routine (sick) visits were conducted when participants presented at the clinic with fever. Both visit types were included in the study, with a total of 407 routine (53 with fever) and 194 non-routine (all with fever) visits (Table 2 and Figure 4g). Venous blood draws were performed into 10-ml EDTA tubes and processed within

24 h on Remoscope using the 10× diluted blood assay with reconstituted diluent. Thick blood smears were fixed, stained with Giemsa and read in duplicate by experienced microscopists. In the event of a disagreement, a third read was performed (as described in Kamya et al.[24]). qPCR targeting the *Pf* multicopy conserved *var* gene acidic terminal sequence was performed on all samples (Figure 4a). Those with positive microscopy but negative qPCR results were additionally processed with a species PCR panel to screen for *Plasmodium ovale* and *Plasmodium malariae* (Figure 4a, h). Remoscope runs were quality vetted according to seven criteria as described above and in Supplementary Figure 5. Datasets with cell counts of <75 600 (the bottom 5th percentile) were also excluded from analysis due to inadequate statistical sampling power.

The cohort had an overall *Pf* prevalence of 67.9% by qPCR, 38.2% by traditional thick blood smear microscopy and 45.4% by Remoscope (Table 3). By qPCR, the cohort's parasitaemia levels were evenly distributed across a logarithmic range spanning from <1 to >600 000 parasites/μl (Figure 4c and Supplementary Video 18). One participant had sickle cell disease, five samples tested positive for *P. ovale* and three tested positive for *P. malariae*, all of which were excluded from our diagnostic analyses (Figure 4h). In all figures, the data were clipped along the x-axis to a value of 1 parasite/μl in order to focus on the range that is relevant to microscopy and Remoscope, as the qPCR LoD is approximately three orders of magnitude lower.[28]

Remoscope's 10× diluted blood assay resulted in an average of 243 623 RBCs per run in the cohort (Figure 4e) and closely tracked the results of expert-level thick smear microscopy performed in duplicate (Figure 4f, h). In Figure 4f, we plot Remoscope and microscopy results vs qPCR. On average, the Remoscope diluted blood assay scans a similar number of cells as viewed by a technician performing microscopy, where the number of asexual parasites per either 200 or 500 leucocytes is counted (the latter for low-density samples), with an assumption of 8000 leucocytes/μl. Therefore thick smear microscopy inspects an equivalent of 125 000–312 500 RBCs, using an average RBC concentration of 5×10^6/μl. Fundamental counting statistics place similar bounds on the performance of Remoscope as microscopy, with microscopy benefitting from the added specificity of stain and duplicate technician readings.

Since qPCR assays for *Pf* have a LoD at least three orders of magnitude lower than either microscopy or Remoscope (estimated at 22 parasites/ml[28,29]), direct comparison of binarized diagnostic outputs with qPCR results in low sensitivity values. Furthermore, detection of subpatent infections in a high-transmission/high-prevalence setting is of limited clinical value when the prevalence regardless of symptoms is 69%. We therefore considered a swept qPCR positivity threshold ranging from 1 to 1000 parasites/μl in order to quantify diagnostic performance statistics (Figure 4i–n) and tabulated a subset in Table 3. We computed sensitivity, specificity, positive predictive value (PPV), negative predictive value (NPV), positive likelihood ratio (+LR) and negative likelihood ratio (−LR) with respect to the common swept positivity threshold.

Remoscope's LoD was computed as the mean plus 3 SD of all qPCR negative samples, resulting in an LoD of 95.1 parasites/μl. By this metric, microscopy had no false positive results. While this suggests an LoD of 0, the method cannot detect arbitrarily small

Table 3. Summary of diagnostic statistics by method and positivity threshold.

Method	Positivity threshold (/μl)	Sensitivity	Sensitivity SEM	Specificity	Specificity SEM	PPV	PPV SEM	NPV	NPV SEM	PLR	NLR	F1	MCC
Microscopy	0	0.54	0.024	1.00	0.00	1.00	0.00	0.50	0.026	∞	0.46	0.70	0.52
Microscopy	1	0.74	0.025	0.99	0.0066	0.98	0.009	0.80	0.021	56.61	0.26	0.85	0.75
Microscopy	95	0.90	0.022	0.99	0.0059	0.97	0.014	0.96	0.010	62.96	0.10	0.93	0.91
Microscopy	200	0.92	0.022	0.98	0.0068	0.94	0.018	0.97	0.008	44.64	0.09	0.93	0.90
Microscopy	300	0.93	0.020	0.97	0.0085	0.91	0.023	0.98	0.007	28.10	0.07	0.92	0.89
Microscopy	500	0.93	0.021	0.96	0.0094	0.87	0.028	0.98	0.007	21.78	0.07	0.90	0.87
Remoscope	0	0.55	0.024	0.78	0.030	0.85	0.022	0.44	0.027	2.46	0.58	0.67	0.30
Remoscope	1	0.71	0.022	0.81	0.029	0.78	0.025	0.74	0.024	3.67	0.36	0.74	0.52
Remoscope	95	0.83	0.019	0.96	0.014	0.91	0.018	0.93	0.014	21.63	0.18	0.87	0.81
Remoscope	200	0.87	0.016	0.99	0.0085	0.96	0.012	0.95	0.012	63.85	0.13	0.91	0.89
Remoscope	300	0.85	0.018	0.99	0.0084	0.96	0.012	0.95	0.012	63.87	0.15	0.90	0.87
Remoscope	500	0.83	0.018	0.98	0.0095	0.93	0.015	0.95	0.012	48.54	0.17	0.88	0.85

SEM: standard error of the mean.
All Remoscope statistics were computed using compensated (linearly transformed) results and a YOGO model confidence threshold of 0.99.

Table 4. Agreement level between microscopy and Remoscope.

Binarized result summary	Microscopy negative	Microscopy positive
Remoscope negative	366	66
Remoscope positive	9	160

A breakdown of the agreement between Remoscope and microscopy for binarized diagnostic results. For Remoscope, a positivity threshold equal to its LoD was used (95.1 parasites/µl), whereas for microscopy a threshold of 0 parasites/µl was used, in concordance with existing clinical practices.

parasitaemia, and the smallest detectable level is then limited by the probability of detection. Using the method outlined by Armbruster and Pry,[30] we computed the limit of blank (LoB) for each method and subsequently the fraction of clinical data points exceeding each method's LoB as a function of the qPCR value (Supplementary Figure 6).

The YOGO model confidence threshold also influenced diagnostic performance, and we computed the metrics for three values: 0.9, 0.95 and 0.99. For example, Remoscope's LoD continued to improve with increasing model confidence thresholds up to a value of 0.99 (Supplementary Figure 7) due to the reduction of false positives and improvement of specificity. The optimal selection of model confidence and positivity threshold is influenced by what is important for clinical decision-making: here we opted to use a value of 0.99 model confidence threshold in order to prioritize specificity and LoD. In Table 3 and Figure 4f–h, a model confidence threshold of 0.99 was employed throughout. We also computed integrated performance metrics such as the F1 score and Matthews correlation coefficient (MCC)[31] as a function of positivity and model confidence thresholds (Supplementary Figure 8). We achieved a maximal MCC value of 0.9 at a model confidence threshold of 0.98 and positivity threshold of 300 parasites/µl.

Remoscope exhibited similar sensitivity and NPV as expert thick smear microscopy across a wide range of positivity thresholds (Table 4 and Figure 4i, l). While microscopy remains superior in specificity and PPV, there is robust evidence that Remoscope's false positive rate is more than 10-fold lower with undiluted blood (Figure 3 and Supplementary Figure 9). Fever status of participants is stratified in Figure 4g and Supplementary Figure 10, showing bias toward higher parasitaemia with fever. In Figure 4h, we plot Remoscope vs microscopy and include other *Plasmodium* species, noting that the YOGO model, untrained on these species, exhibited a partial sensitivity to the parasites. See Supplementary Figure 11 for example images of non-*Pf* parasites.

Discussion

In this pilot study we introduced the Remoscope platform and demonstrated its utility as a diagnostic instrument for malaria in a clinic in eastern Uganda, comparing performance to thick smears and qPCR. The base cost of the instrument and disposable flow cartridges are within the means of endemic countries, and future work will characterize the direct and indirect cost-effectiveness of the platform's deployment in clinics. We evaluated Remoscope's use in laboratory research applications by showing that parasitaemia quantification is linear across a 16-point dilution series. We also showed that treatment of *Pf* parasite cultures with CQ imparted sufficient morphological changes to evade detection by a custom trained convolutional neural network, enabling EC_{50} drug evaluations in vitro.

In comparison with traditional Giemsa microscopy (using qPCR as the gold standard), Remoscope exhibited similar sensitivity and PPV but lower specificity and NPV. It should be noted that the manual smear readout in this study was expert level and performed in duplicate with research-grade reagents, resulting in performance not achieved in lower-tier health facilities. In fact, it has been shown that even at 100 parasites/µl the average probability of detection by microscopists in clinical settings globally is $<30\%$.[12] Thus Remoscope's diluted blood assay already exceeds the average standard of care. Examination of Remoscope false positives revealed the primary causes to be deformed RBCs and debris stuck to the flow cartridge surface. Despite vetting efforts (Figure 4a), it is likely that inconsistent diluent reconstitution affected RBC morphologies. With undiluted blood, a 10-fold improvement in the LoD is anticipated, along with improvements to other metrics. The benefits of undiluted blood have been validated in vitro with a parasite titration to 17.1 parasites/µl, as well as an average false positive rate of 3 parasites/µl based on a small cohort of healthy donors (Supplementary Figure 9). Future clinical studies will aim to validate these advantages in performance and workflow.

An additional consideration is the rigidity and cytoadherence properties of *Pf* schizonts,[32,33] which renders them more likely to be trapped inside our prototype flow cartridge upstream of the imaging window, failing detection. Our life stage analysis (Figure 3) showed a decrease in mature schizont detection efficiency. Fortunately, since most clinical *Pf* samples contain primarily rings, as more mature stages are not circulating, this phenomenon is not expected to impact clinical performance. We also observe intermittent adhesion of white blood cells (WBCs) to the flow cartridge, straddling the requirement that RBCs lay flat for imaging while not clogging larger cell types. In some cases, the diagnosis was hampered by high WBC counts and rejected during the vetting process. Future flow cartridge designs will employ hydrodynamic flow focusing[34] to confine blood to a freely flowing monolayer while permitting unbiased flow and counting of all cell types, including late stages of *Pf*, while also enabling a wide array of other low-cost cytometry applications beyond the detection of malaria.

In this work, only models to detect *Pf* were trained, as it is the species responsible for the large majority of malaria cases and deaths worldwide[1] and is amenable to lab culture. Expanding into other species is a logical continuation of this work, as there are regions where other *Plasmodium* species such as *P. vivax* are prevalent and identification of species information is crucial to informing treatment as well as epidemiological tracking in certain geographic regions. In our clinical cohort, we observed a small number of *P. ovale* and *P. malariae* cases (Supplementary Figure 11). Our model achieved partial

cross-species detection, despite no training examples of non-*Pf* parasites (Figure 4h).

The image data from this study have been made freely available as a resource to the community. To our knowledge, this resource represents the largest collection of label-free live parasite images ever produced, consisting of 14.4 million images and 399 million blood cells from healthy donors, infected patients and cultured parasites. This collection of images provides a rich set of data for machine learning and evolving artificial intelligence approaches. In addition to further development for malarial diagnostics, future efforts will expand the application space of high-throughput, low-cost scanning of blood morphology to other bloodborne pathogens (such as trypanosomiasis or babesiosis), hereditary blood disorders such as sickle cell disease (Supplementary Figure 12), complete blood counts and morphological fingerprinting of RBC ensembles using more generalized machine learning frameworks. These expansions in throughput and model complexity will be well-supported by a favourable trend in portable computing hardware performance without increasing cost.

Supplementary data

Supplementary data are available at *Transactions* online.

Authors' contributions: PML led the project. CC and PML designed and built the optics and hardware with assembly help from PCF, WW and JD. EH designed the custom electronics. MWLK, AJ and IJ developed instrument control and data analysis software with PML. CC and PML developed the flow cartridges. PML, CC, AJ, EH and PCF developed the flow cartridge quality control system. WW fabricated and performed quality control on the flow cartridges. AS, PML and AJ performed image annotation. A.S. performed parasite culture, titrations, life stage experiments and drug studies. YOGO was developed and deployed by AJ. JE collected clinical cohort data and assisted with data preprocessing by GD. RGS and JD provided guidance and advisory support for the project. PML wrote the manuscript with assistance from MWLK, IJ, AJ and AS.

Acknowledgements: The authors would like to express their gratitude to the many members of the Infectious Disease Research Collaboration who helped facilitate the project. We would also like to acknowledge Dr Georgios Batsios for assisting with lyophilization of the diluent.

Funding: This work was supported by the Chan Zuckerberg Biohub San Francisco.

Competing interests: PML, RGS and JLD declare international patent application PCT/US2021/047974. The remaining authors declare no conflicts of interest.

Ethical approval: All research was conducted in accordance with local regulatory requirements and approvals. Blood was drawn at the University of California, San Francisco (UCSF) from healthy adult volunteers providing written consent for use in sustaining malaria cultures and imaging of healthy blood under UCSF IRB#10-02381. Approval for the Ugandan cohort study was obtained from the Makerere University School of Medicine Research and Ethics Committee (REF 2019-134), the Uganda National Council of Science and Technology (HS 2700), the London School of Hygiene and Tropical Medicine Ethics Committee (17777) and the University of California, San Francisco Committee on Human Research (257790). Written informed consent was obtained from all participants prior to enrolment in the study. Funding was provided by the National Institutes of Health as part of the International Centers of Excellence in Malaria Research program (U19AI089674).

Data availability: The raw images and annotations supporting the findings of this study are hosted on the BioStudies image server under study number S-BIAD1623 (https://www.ebi.ac.uk/biostudies/bioimages/studies/S-BIAD1623). All the processed numerical data contained in the figures is provided as supplementary material. All software and machine learning models are provided in public GitHub repositories (see below). Tables of data for Figures 3 and 4 are provided as Supplementary Data 1 and Supplementary Data 2, respectively, and a concise table of all clinical results and metadata is included as Supplementary Data 3.

Code availability: All software developed for this project is open source and publicly available: instrument control software (https://github.com/czbiohub-sf/ulc-malaria-scope), YOGO (https://github.com/czbiohub-sf/yogo), data analysis utilities (https://github.com/czbiohub-sf/lfm-data-utilities), statistical analysis (https://github.com/czbiohub-sf/remo-stats-utils) and single-shot autofocus (https://github.com/czbiohub-sf/ulc-malaria-autofocus).

References

1 World Health Organization. World malaria report 2024: addressing inequity in the global malaria response. Geneva: World Health Organization; 2024.

2 Mnzava A, Monroe AC, Okumu F. *Anopheles stephensi* in Africa requires a more integrated response. Malar J. 2022;21:156.

3 Emiru T, Getachew D, Murphy M, et al. Evidence for a role of *Anopheles stephensi* in the spread of drug- and diagnosis-resistant malaria in Africa. Nat Med. 2023;29(12):3203–11.

4 Poostchi M, Silamut K, Maude RJ, et al. Image analysis and machine learning for detecting malaria. Transl Res. 2018;194:36–55.

5 Krampa FD, Aniweh Y, Awandare GA, et al. Recent progress in the development of diagnostic tests for malaria. Diagnostics. 2017;7(3):54.

6 Barcia JJ. The Giemsa stain: its history and applications. Int J Surg Pathol. 2007;15(3):292–6.

7 Nankabirwa JI, Yeka A, Arinaitwe E, et al. Estimating malaria parasite prevalence from community surveys in Uganda: a comparison of microscopy, rapid diagnostic tests and polymerase chain reaction. Malar J. 2015;14:528.

8 Gatton ML, Chaudhry A, Glenn J, et al. Impact of *Plasmodium falciparum* gene deletions on malaria rapid diagnostic test performance. Malar J. 2020;19:1.

9 Dalrymple U, Arambepola R, Gething PW, et al. How long do rapid diagnostic tests remain positive after anti-malarial treatment? Malar J. 2018;17:228.

10 Mayxay M, Pukrittayakamee S, Chotivanich K, et al. Persistence of *Plasmodium falciparum* HRP-2 in successfully treated acute falciparum malaria. Trans R Soc Trop Med Hyg. 2001;95(2):179–82.

11 Grabias B, Essuman E, Quakyi IA, et al. Sensitive real-time PCR detection of *Plasmodium falciparum* parasites in whole blood by erythrocyte membrane protein 1 gene amplification. Malar J. 2019;18:116.

12 Slater HC, Ross A, Felger I, et al. The temporal dynamics and infectiousness of subpatent *Plasmodium falciparum* infections in relation to parasite density. Nat Commun. 2019;10:1433.

13 Lai MY, Lau YL. Two-stage detection of *Plasmodium* spp. by combination of recombinase polymerase amplification and loop-mediated isothermal amplification assay. Am J Trop Med Hyg. 2022;107(4):815–9.

14 Abanades B, Georges G, Bujotzek A, et al. ABlooper: fast accurate antibody CDR loop structure prediction with accuracy estimation. Bioinformatics. 2022;38(7):1877–80.

15 Selvarajah D, Naing C, Htet NH, et al. Loop-mediated isothermal amplification (LAMP) test for diagnosis of uncomplicated malaria in endemic areas: a meta-analysis of diagnostic test accuracy. Malar J. 2020;19:211.

16 Morris U, Aydin-Schmidt B. Performance and application of commercially available loop-mediated isothermal amplification (LAMP) kits in malaria endemic and non-endemic settings. Diagnostics. 2021;11(2):336.

17 Das D, Vongpromek R, Assawariyathipat T, et al. Field evaluation of the diagnostic performance of EasyScan GO: a digital malaria microscopy device based on machine-learning. Malar J. 2022;21:122.

18 Yang D, Subramanian G, Duan J, et al. A portable image-based cytometer for rapid malaria detection and quantification. PLoS One. 2017;12(6):e0179161.

19 Li H, Soto-Montoya H, Voisin M, et al. Octopi: open configurable high-throughput imaging platform for infectious disease diagnosis in the field. Biorxiv. 2019:684423. doi: https://doi.org/10.1101/684423

20 Noul. Decentralized diagnostic platform, miLab^{TM}. 2025. Available from: https://noul.com/en/milab/ [accessed].

21 Lebel P, Dial R, Vemuri VNP, et al. Label-free imaging and classification of live *P. falciparum* enables high performance parasitemia quantification without fixation or staining. PLoS Comput Biol. 2021;17(8):e1009257.

22 George-Gay B, Parker K. Understanding the complete blood count with differential. J Perianesth Nurs. 2003;18(2):96–114; quiz 115–7.

23 Kim CC, Wilson EB, DeRisi JL. Improved methods for magnetic purification of malaria parasites and haemozoin. Malar J. 2010;9:17.

24 Kamya MR, Nankabirwa JI, Arinaitwe E, et al. Dramatic resurgence of malaria after 7 years of intensive vector control interventions in Eastern Uganda. PLoS Glob Public Health. 2024;4(8):e0003254.

25 Buderer NM. Statistical methodology: I. Incorporating the prevalence of disease into the sample size calculation for sensitivity and specificity. Acad Emerg Med. 1996;3(9):895–900.

26 David PH, Hommel M, Miller LH, et al. Parasite sequestration in *Plasmodium falciparum* malaria: spleen and antibody modulation of cytoadherence of infected erythrocytes. Proc Natl Acad Sci USA. 1983;80(16):5075–9.

27 Lee W-C, Russell B, Rénia L. Sticking for a cause: the falciparum malaria parasites cytoadherence paradigm. Front Immunol. 2019;10:1444.

28 Ballard E, Wang CYT, Hien TT, et al. A validation study of microscopy versus quantitative PCR for measuring *Plasmodium falciparum* parasitemia. Trop Med Health. 2019;47:49.

29 Imwong M, Hanchana S, Malleret B, et al. High-throughput ultrasensitive molecular techniques for quantifying low-density malaria parasitemias. J Clin Microbiol. 2020;52(9):3303–9.

30 Armbruster DA, Pry T. Limit of blank, limit of detection and limit of quantitation. Clin Biochem Rev. 2008;29(Suppl 1):S49–52.

31 Chicco D, Jurman G. The advantages of the Matthews correlation coefficient (MCC) over F1 score and accuracy in binary classification evaluation. BMC Genomics. 2020;21:6.

32 Sherman IW, Eda S, Winograd E. Cytoadherence and sequestration in *Plasmodium falciparum*: defining the ties that bind. Microbes Infect. 2003;5(10):897–909.

33 Marchiafava E, Bignami A. Sulle Febbri Malariche Estivo-Autunnali. Rome: Innocenzo Artero, 1892.

34 Golden JP, Justin GA, Nasir M, et al. Hydrodynamic focusing—a versatile tool. Anal Bioanal Chem. 2012;402:325–35.